International Journal of Heat and Mass Transfer 126 (2018) 1104–1110

Contents lists available at ScienceDirect

International Journal of Heat and Mass Transfer

journal homepage: www.elsevier.com/locate/ijhmt

Non-equilibrium microsecond pulsed spark discharge in liquid as a source of pressure waves

Nathaniel D. Taylor [a,b], Gregory Fridman [b], Alexander Fridman [a,b], Danil Dobrynin [b,*]

[a] Department of Mechanical Engineering and Mechanics, Drexel University, Philadelphia, PA 19104, USA
[b] C&J Nyheim Plasma Institute at Drexel University, Camden, NJ 08103, USA

ARTICLE INFO

Article history:
Received 19 September 2017
Received in revised form 18 April 2018
Accepted 28 April 2018
Available online 29 May 2018

Keywords:
Pulsed pressure
Spark
Plasma
Pressure wave generator
Water
Fast imaging
Schlieren imaging
Compression
Compressor
Waves

ABSTRACT

The present study investigated the ability of non-equilibrium microsecond pulsed spark discharge in liquid to generate pressure waves and the application of these waves as a source of small-scale compression. The spark pressure wave generator utilized the pressure waves produced by high energy pulsed spark discharge in water to produce usable pressure output in the form of a piston. Pin-to-pin spark generated inside of distilled water was observed in experiments to determine the spark temperature, pressure wave speed and pressure, water displacement, and piston output pressure and frequency. Pressure of 1.87 atm was produced by the piston from a pressure wave pressure of 6.15×10^5 atm generated by the 5500 K temperature spark. These results indicate that spark in water can be used as a source of small-scale compression.

© 2018 Elsevier Ltd. All rights reserved.

1. Introduction

The size limitations of currently available small-scale reciprocating compressors present an opportunity to explore fundamentally new methods of pressure generation with a goal of serving the needs of mobile applications where the pressure requirements are on the order of 1–10 atm. Portable devices which require compression can be reduced in size in part by reducing the size of the compressor but the compressor size is limited by its mechanical components. Comparable size piston and diaphragm pumps produced by G.D. Thomas, KNF, and Hargraves original equipment manufacturers produce pressures of 1–8.2 atm and weigh 200–2132 g [1–3]. The markets for these pumps and compressors as stated by Hargraves and KNF, include in part, environmental monitoring, medical devices, patient monitoring, and medical therapy [4,5].

One potential solution to reducing the size of these compressors are microfluidic valves and micropumps. These devices use microelectromechanical systems (MEMS) technology for application in a variety of fields that include drug delivery, microelectronic cooling, and blood transport [6,7]. In a review of micropumps by Laser and Santiago, the max pressure change possible out of the 47 devices reviewed was 3 atm and the average pressure change was 0.25 atm [7]. Based on this pressure generation, micropumps are not capable replacing existing small-scale compressors but instead serve to fill the needs of newly developed MEMS technologies.

Microsecond spark discharge produces temperatures near the spark channel of 10,000–20,000 K at atmospheric pressure in less than 5 μs that result in the production of intense pressure waves outward from the channel [8,9]. Studies into using spark discharge in water as a source of pressure waves have been previously conducted for the inactivation of bacteria, gallstone fragmentation, removal of calcium carbonate in water, and the formation of sheet metal, but has never been utilized as a method of compression before [10–13]. The study presented here is focused on studying the pressure waves generated by spark in water and the development of a device to produce usable pressure of 1–20 atm from a system that uses limited mechanical components.

2. Materials and methods

Experiments were conducted in a plastic discharge chamber that housed the electrodes and water. This chamber was connected

* Corresponding author.
E-mail address: danil@drexel.edu (D. Dobrynin).

https://doi.org/10.1016/j.ijheatmasstransfer.2018.04.160
0017-9310/© 2018 Elsevier Ltd. All rights reserved.

to a resistor–capacitor (RC) circuit to generate the spark pulses. Fig. 1 shows a schematic diagram of the testing configuration which consists of an RC circuit, adjustable spark gap, discharge chamber, voltage probe, current probe, and oscilloscope. The RC circuit contains a Bertan 205A-50R 50 kV DC power supply, 100 kΩ resistor, and 6800 pF capacitor bank. To monitor the spark discharge electrical parameters, the voltage and current were measured using a Tektronix P6015A 1:1000 75 MHz high voltage probe, Pearson 4100 1 V/A current probe with 10 ns usable rise time, and a 1-GHz Tektronix DPO4000B digital phosphor oscilloscope with an impedance of 1 MΩ ±1%.

Sparks were generated within the discharge chamber shown in the schematic in Fig. 2. This chamber was 3D printed out of ABS plastic using a MakerBot Replicator 1 and Servometer metal bellows were attached to the top. The electrodes entered through the chamber walls and were held in place by threaded metal inserts. The internal volume of chamber that contains the water is a cylinder with final dimensions of 9.88 mm diameter and 17.25 mm depth.

The bellows were used to provide a means of observing the pressure output in place of a typical piston which would be used in a reciprocating compressor. The bellows are hollow inside, sealed on one end, and open to the chamber on the other end. The bellows are electroformed nickel and have a spring rate of 1033 N/m, inner diameter of 3.81 mm, and a maximum stroke length of 2.82 mm as specified by the manufacturer [14]. The chamber and bellows were filled with approximately 2 ml of distilled water and sealed so that no air bubbles were present. Distilled water was used as opposed to tap water to reduce the mineral content in the water to prevent mineral fouling inside of the device. Throughout testing with distilled water, no mineral fouling was observed.

The water was changed before and after each experiment so that any effects caused by changing water chemistry were minimized. The changes in water chemistry were not measured during this study but products generated by plasma in water have been observed by Mededovic and Locke to produce stable H_2O_2, H_2, and O_2 [15]. Over time these chemical products will increase the acidity and chemical composition of the water enough to change the breakdown conditions of the water. Long duration tests were not conducted but during experiments over 1 h at a pulse frequency of 1 Hz would produce noticeable changes in spark frequency. To run the system continuously at a consistent pulse frequency, the water should be changed approximately every 10 min.

The electrodes were constructed out of 316 stainless steel bolts to provide adjustability and were machined to a tip diameter of 0.6 ± 0.1 mm to provide electric field enhancement. The distance between the electrodes was set to 0.9 ± 0.1 mm which was the largest distance possible with the most consistent discharge pulses observed. The gap between the electrodes changes the amount of energy which is deposited into the water because a smaller gap requires less voltage to reach breakdown conditions. As the distance between the electrodes increases, more energy is required to ionize the water between the electrodes. It was observed experimentally that as the circuit operates at higher discharge voltage, the frequency of the spark being generated by the circuit become less consistent.

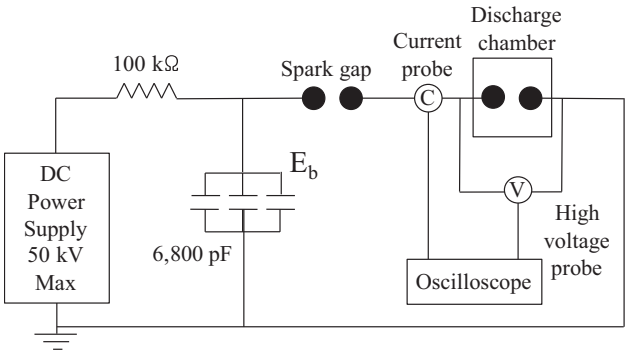

Fig. 1. Schematic diagram of the spark generation testing configuration.

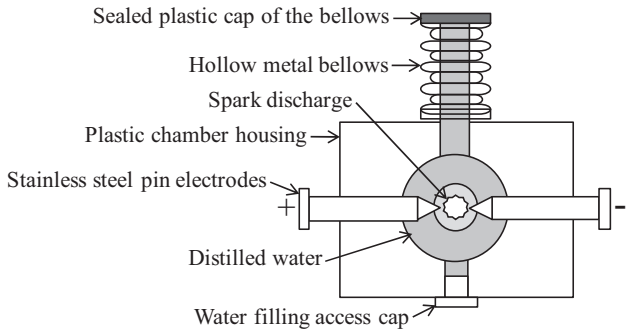

Fig. 2. Schematic diagram of the discharge chamber.

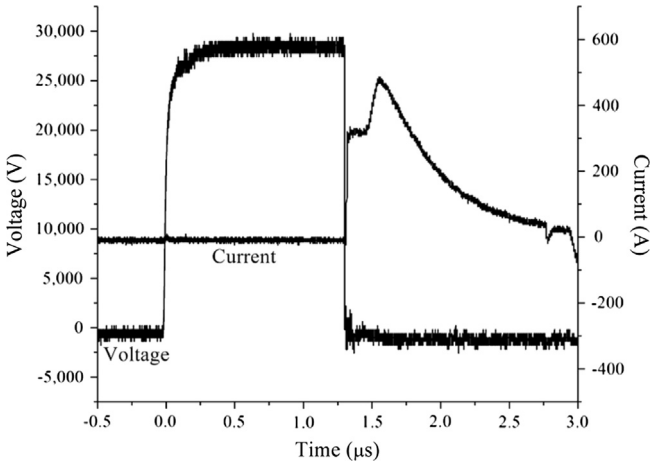

Fig. 3. Oscillogram of the voltage and current for a typical spark discharge in water.

Fig. 3 shows an oscillogram of the voltage and current of a typical spark discharge pulse. The peak-to-peak voltage and current ranged from 25 to 40 kV and 400 to 900 A respectively. The pulse width ranged from 1 to 5 μs and the voltage rise time was approximately 40 ns. The pulse energy was calculated by integrating the voltage and current over the pulse width.

2.1. Pressure output tests

The metal bellows were used to measure the average volume displaced by the spark, the pressure output of the device, and to determine the potential piston stroke generated. Measurements of the bellows were conducted using high speed imaging with a Phantom Miro M310 high speed video camera with a 1 μs exposure time. Images were extracted from the videos and the displacement of the bellows were measured with ImageJ software using a known pixel length.

2.2. Pressure wave observation tests

Schlieren imaging was utilized for imaging the spark discharge and pressure wave formation. Fig. 4 shows a schematic of the Sch-

lieren imaging setup used that was based on dual-field-lens arrangement detailed by G.S. Settles [16]. Images were captured using a Stanford Computer Optics 4Picos ICCD camera with a minimum exposure of 200 ps. An Oriel 60,000 series arc lamp with adjustable power supply that can provide 50–200 W was used as a light source. The chamber was modified to include glass windows on each side to let the light pass through to observe the discharge region. The diameter of the chamber was increased from 12 mm to 26.6 mm to accommodate the windows. The lamp, lenses, chamber, camera, and razor were all attached to an optical table to prevent misalignment and movement of any of the components.

The camera was triggered using the signal from a Tektronix P6015A high voltage probe connected after the spark gap in the circuit shown in Fig. 1. Following the spark gap, approximately 304 m of coaxial cable was used to create a time delay of the pulse before it reached the discharge chamber. This delay was required to capture the discharge because the camera has a minimum internal camera trigger propagation delay specified by the manufacturer of 65.4 ± 0.2 ns in addition to any signal delays from the voltage probe and the 3 m coaxial cable connecting the probe to the camera input. The delay generated by the long coaxial cable was measured to be 1.436 μs using the oscilloscope and a Tektronix P6015A high voltage probe at each end of the 304 m coaxial cable.

2.3. Temperature measurement by OES

The optical emission spectrum (OES) of the discharge was obtained using a Princeton Instruments Acton 10 fiber 200 μm core bundle connected to a Princeton Instruments TriVista TR555 spectrometer with a PIMAX digital ICCD camera. The spectrometer camera was triggered in the same manner as the 4Picos camera. The spectrometer was calibrated before conducting experiments using a Oriel 6035 Hg(Ar) calibration lamp. No background subtraction was necessary since the emission from the spark is much greater than the background. Temperature of the spark was calculated using the relative emission intensities of spectral lines using the Boltzmann plot technique and Eq. (1) [17–19].

$$\ln\left(\frac{I_{ij}\lambda}{g_k A_{ki}}\right) = -\frac{E_k}{k_B T_{exc}} + C \tag{1}$$

where I_{ij} is the relative intensity of the emission line, λ_{ij} is the wavelength, g_k is the upper level statistical weight, A_{ki} is the emission transition probability, E_k is the upper level energy, k_B is the Boltzmann constant, T_{exc} is the excitation temperature, and C is a constant.

3. Results and discussion

3.1. Spark discharge in water and bubble generation

Images of the discharge initiation and subsequent bubble formation are shown in Fig. 5. These were captured at a 200 ns exposure time and the frames are labeled with the elapse time after camera triggering. Each image represents a different spark pulse at a different delay time from the camera trigger point in order to obtain observe the propagation of the wave. Experiments were repeated 3 times to obtain the experimental error of the wave propagation. Spark discharge starts around 2 μs when a bubble begins to form between the pin electrodes. The bubble formation is followed by the generation of an energetic microsecond spark at around 5 μs. After the discharge, a vapor bubble remains and continues to expand radially outward from the electrodes as a result of heating.

There is not yet a consensus on the initiation of mechanism of plasma in water but has been well documented by Yang to be consisting of two groups of thought. One group believes that heating in the electric field at the electrodes generates bubbles which allows the plasma to breakdown inside of the formed bubble. The other group believes that plasma in water is initiated by partial discharge without bubbles where high current is transferred by ions [9]. Despite the initiation mechanism, both methods will generate bubbles as discharge starts to form and heating increases from the increase in current.

Fig. 5 shows that the bubble collapses and eventually disappears before the next discharge forms. It can also be seen in Fig. 5 that small bubbles are generated and remain in the water outside of the region between the electrodes. These can be seen most clearly in the 205, 400, and 500 μs images. The maximum bubble radius was measured from the images using ImageJ software to be 3.75 ± 0.09 mm and grows at a velocity of 1.83 m/s from 100 to 200 μs. Based on this radius, the volume displaced by this bubble was estimated to be 221 mm^3. This calculated volume doesn't account for the electrode tips that enter slightly through the sides of the bubble.

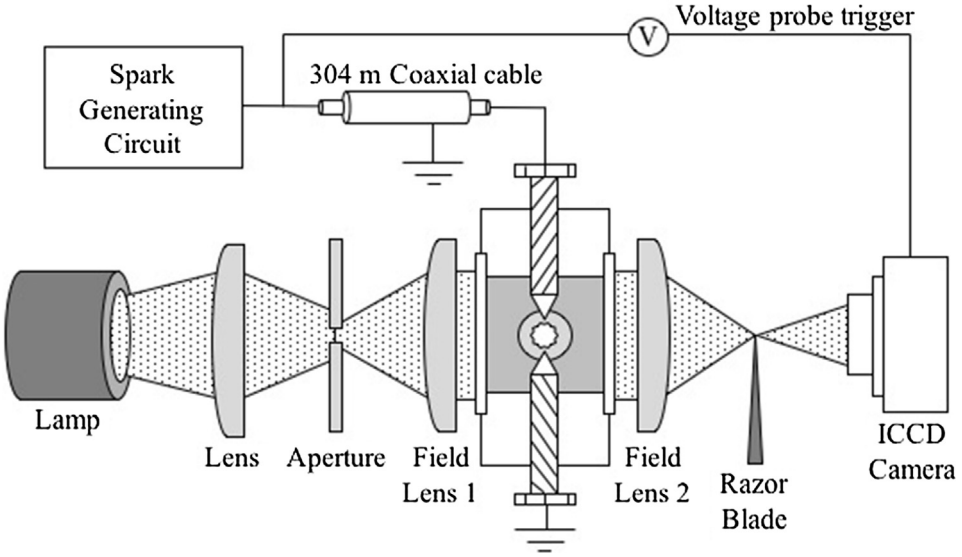

Fig. 4. Schematic of the dual-field-lens Schlieren arrangement for imaging pressure waves.

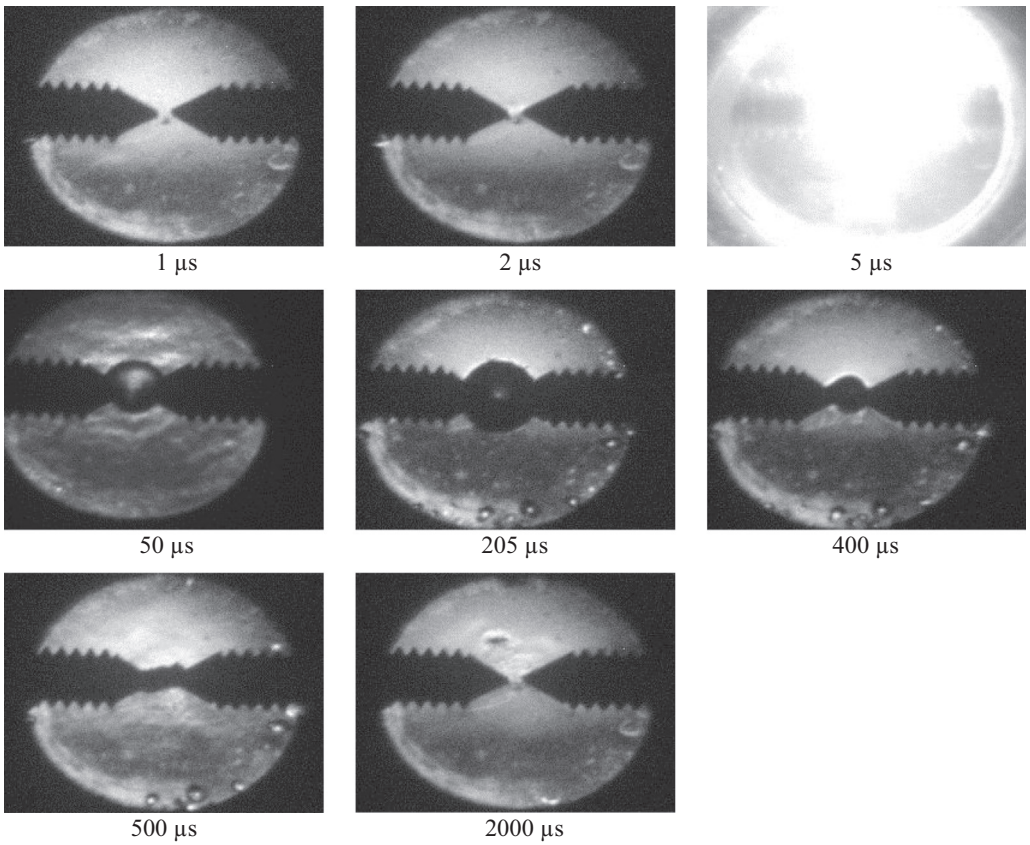

Fig. 5. Images of spark initiation followed by the bubble growth and collapse over time.

3.2. Pressure wave formation

Images of the pressure wave propagation are shown in Fig. 6. These were captured at a 2 ns exposure time and the velocity of the wave was measured using ImageJ software. The change in the pressure wave radius over the 100 ns time between frames was calculated to be 11.9 km/s from 5 to 5.1 μs from an input energy of 0.087 ± 0.001 J/pulse. This is significantly larger than the sound velocity in water of 1485 m/s that was calculated at a room temperature of 21 °C using Eq. (2) where T is the liquid temperature [20]. The velocity from 5.1 to 5.2 μs was much lower at 2.21 km/s. After 5.2 μs the pressure wave was no longer visible due to the increased brightness of the spark and the initial pressure wave reaching the chamber wall. The measurements of the pressure waves are provided in Table 1.

$$c = 1404.4 + 4.7T - 0.04T^2 \quad (2)$$

The pressure generated by the pressure wave was calculated to be 6.15×10^5 atm for 11.9 km/s and 7.91×10^3 atm for 2.21 km/s using Eq. (3) [21]. These pressures are similar to the 1×10^4 atm which was measured in previous work done on underwater streamer pressure [22].

$$P = \rho_0 u_s \frac{u_s - A}{B} \quad (3)$$

where u_s is the pressure wave velocity, A is the sound velocity in water, and B is a constant of 1.99 [21].

3.3. Optical emission spectroscopy

The full spectrum obtained of the spark discharge in water indicates strong Hα, singlet oxygen, and iron atomic spectra lines as shown in Fig. 7. The iron emission lines used for temperature measurements are shown in Fig. 8. Plasma temperature of the discharge was calculated to be 5500 ± 608 K from the Boltzmann plot method shown in Fig. 9 using the values in Table 2 [23,24]. This value is consistent with the temperature results reported by Anpilov for electric spark in water with temperatures of 4000–5000 K [25].

3.4. Displacement of the bellows

Images of the vertical displacement of the bellows are shown in Fig. 10 and were captured at a 68.66 μs exposure time with an 86.27 μs interval time between images. After the initial maximum extension of the bellows, they oscillated for several milliseconds. This oscillation was produced by the restoring force from the bellows' spring force as shown in Fig. 11.

The displacement of the bellows at different input energy is shown in Fig. 12 with the maximum displacement ranging from 0.70 ± 0.01 mm to 0.94 ± 0.02 mm. Since water is essentially an incompressible fluid, it is only possible that the bellows are able to be compressed below the initial position because of the presence of bubbles which are generated during the spark discharge. The liquid turns into gas bubbles as shown in Fig. 5 and provides compressible volumes of gas throughout the water volume. The largest of these bubbles eventually collapse and the gas reabsorb into the water. The volume displaced inside of the bellows from the initial to max position was calculated to be 7.9 ± 0.23 mm^3 to 10 ± 0.11 mm^3 based on the internal dimensions of the bellows. These volumes are significantly smaller than that of the 221 mm^3 bubble generated at the electrodes. Based on the relatively long time required for the extension of the bellows compared to the short duration of the electrode bubble expansion and collapse, it

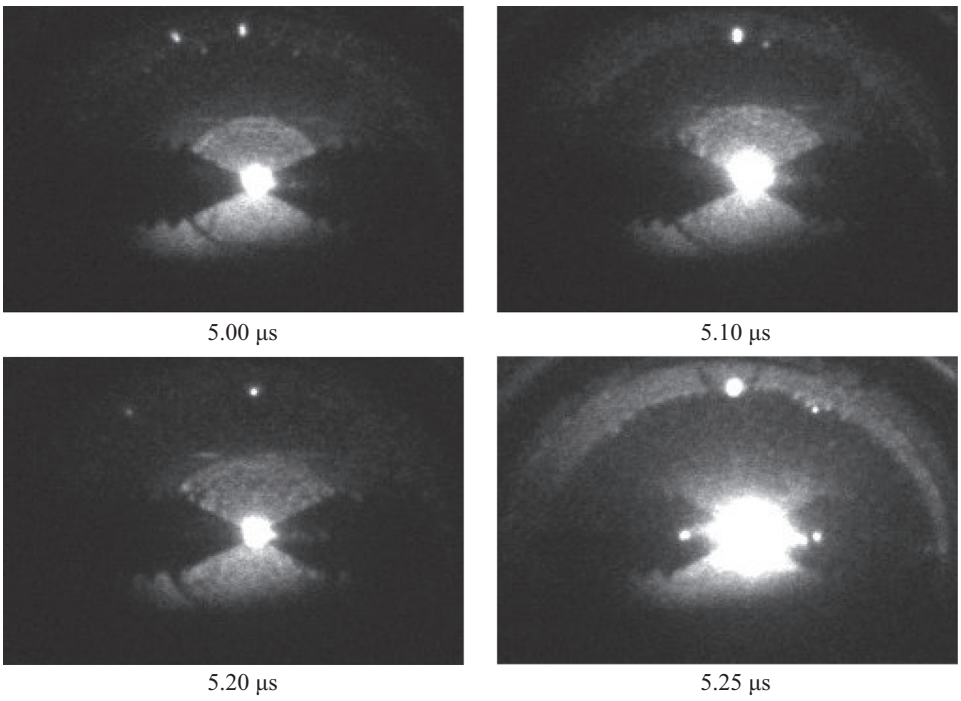

Fig. 6. Images of the pressure wave propagation over time.

Table 1
Measured radii and calculated velocities of pressure waves in water.

Time (μs)	Pressure wave radius (mm)	Standard deviation (mm)	Velocity (km/s)
5.00	4.91	0.31	
5.10	6.10	0.13	11.9
5.20	6.33	0.32	2.21

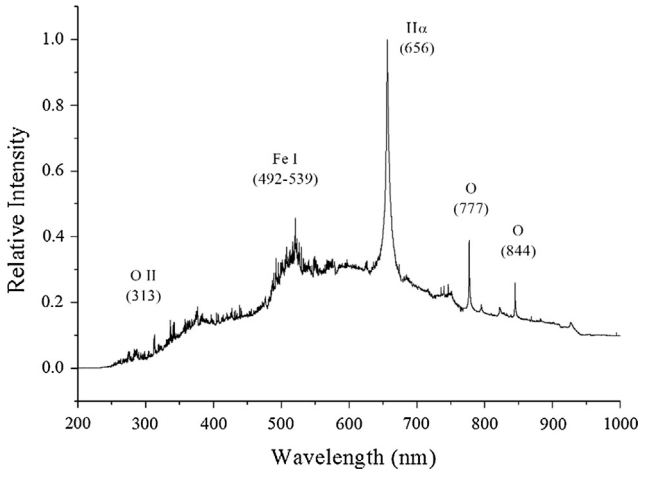

Fig. 7. Plot of the full spectrum obtained for spark discharge in water.

is believed that the compression of the bellows is possible because of the distributed small bubbles in the water volume within the chamber.

The average pressure generated in the system was estimated using Hooke's law of spring motion $F = kX = PA$, where F is the force exerted by a spring, k is the spring constant, X is the spring extension distance, P is pressure, and A is area of contact surface. The pressure was calculated using the distance that the bellows

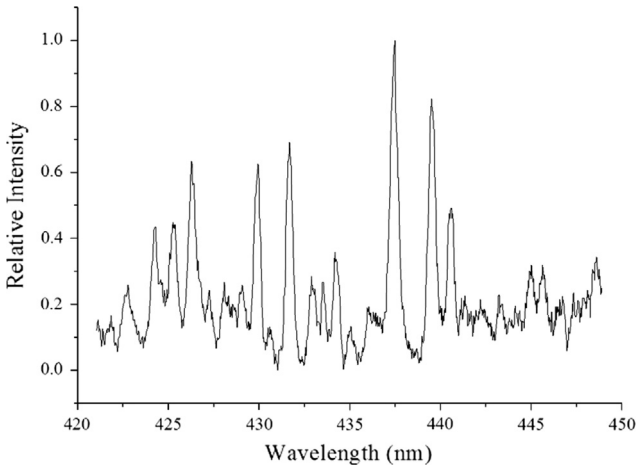

Fig. 8. Plot of the partial spectrum obtained for spark discharge in water showing Fe I atomic emission lines.

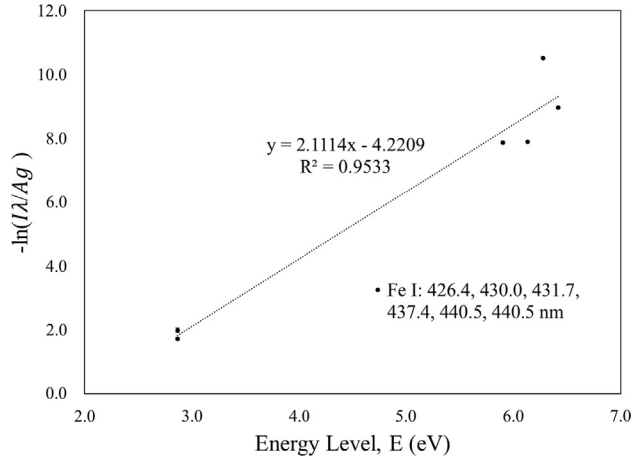

Fig. 9. Boltzmann plot for Fe I was used to calculate the plasma temperature of the spark.

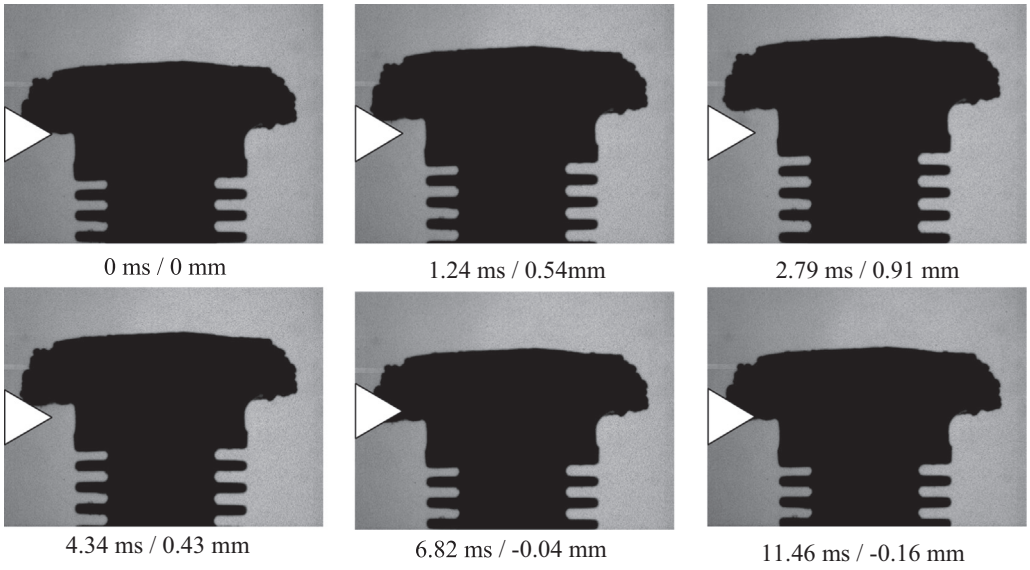

Fig. 10. Images of the displacement of the bellows over time.

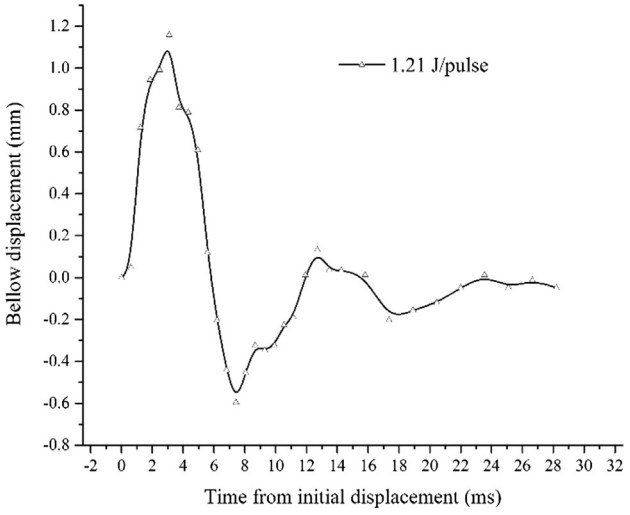

Fig. 11. Plot of the vertical displacement of the metal bellows.

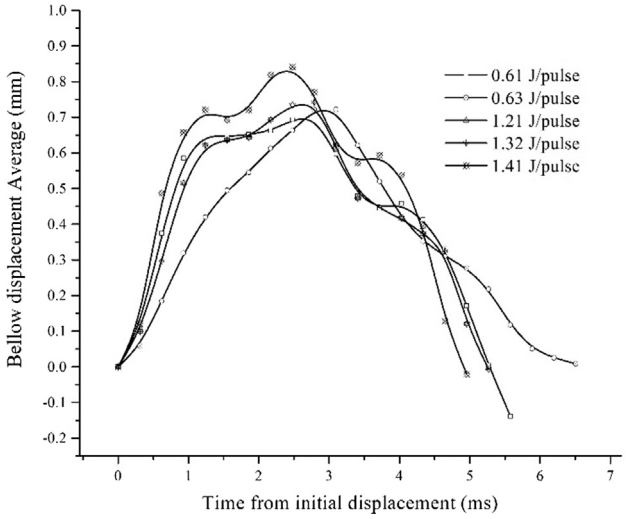

Fig. 12. Plot of the vertical displacement of the bellows from a single spark at different energy inputs.

travel from Fig. 12 and the internal surface area of the bellows' cap which is exposed to the force of the water. The pressures were calculated to be 0.65 ± 0.02 atm to 0.87 ± 0.01 atm for input energies of 0.61 ± 0.03 J/pulse to 1.41 ± 0.03 J/pulse, respectively. From the displacement of the bellows shown in Fig. 11, it was determined that the bellows operate at a frequency of 143 Hz to complete one cycle.

3.5. High frequency pulses

The circuit in Fig. 1 was modified using a variable frequency power supply to increase the spark frequency from a 1 Hz to a maximum of 26.5 Hz. At a voltage frequency input of 26.5 Hz, the output frequency of the bellows was 14 Hz at the peak height

Table 2
Fe I atomic spectra line data used to create the Boltzmann plot [24].

Wavelength, λ	Transitional probability, A_{ki}	Upper energy level, E_k (eV)	Upper statistical weight, g_k	Average relative intensity, I_{ij}	Standard deviation
426.4	1.62E+06	6.2749966	7	0.7142	0.0315
430.0	2.65E+05	5.9004139	3	0.7043	0.0463
431.7	5.20E+05	6.4176794	5	0.7654	0.0211
437.4	1.68E+05	6.1343819	7	1.0000	0.0000
440.5	2.95E+02	2.8653912	7	0.8344	0.0313
440.5	2.95E+02	2.8653912	7	0.6412	0.0722

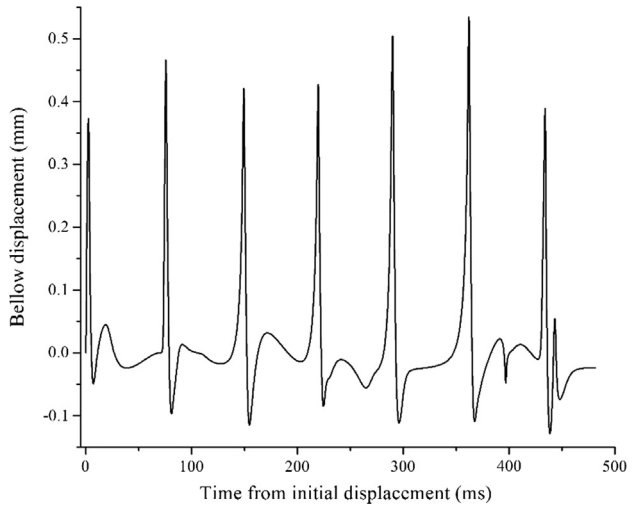

Fig. 13. Plot of the vertical displacement of the metal bellows from a 26.5 Hz spark input.

as shown in Fig. 13. The output frequency of the bellows didn't match the input frequency of the spark due to not being synchronized. The frequency of the bellows could be increased if the spark was synchronized with the frequency of the bellows' motion.

4. Conclusions

The present study investigated the ability to produce pressure waves by microsecond spark discharge in water. It was reported that pressure waves generated by the intense heat of a microsecond spark can produce 6.15×10^5 atm of pressure at the spark channel. This pressure can be constrained into a mechanical compressor using metal bellows. It was also reported that the bellows can output a pressure of 1.87 atm and are capable of operating at a frequency of 14 Hz without synchronization. These results indicate that spark in water can be used as source of small-scale compression without the need for mechanical components which reduces the size and complexity of the compressor and has the potential to increase the lifespan of small-scale compressors. Technological challenges to the lifespan of this device primarily are the chemical stability of the water and electrode erosion. To overcome the challenge of water chemistry, other liquids could be explored or a system of replacing the water could be implemented. Electrode erosion was not a limiting factor during this study and similar electrodes have been shown by Yang to operate continuously for over 50 h at a frequency of 1 Hz [26]. The lifetime of the electrodes could be extended beyond this through the use of larger radius electrodes and harder materials such as tungsten.

Conflict of interest

None.

References

[1] KNF, 2016, January 28, 2016, OEM pumps. Available: <http://www.knfusa.com/products/oem-pumps/>.
[2] Hargraves, 2008, January 23, 2016, Air & gas pumps. Available: <https://www.hargravesfluidics.com/air_pumps.php>.
[3] G.D. Thomas, 2016, January 23, 2016. Compressors and vacuum pumps. Available: <http://www.gd-thomas.com/compressors-and-vacuum-pumps/>.
[4] H.M. Served, 2008, January 30, 2018, Air & gas pumps. Available: <https://www.hargravesfluidics.com/markets.php>.
[5] KNF, January 30, 2018, OEM pump applications. Available: <https://www.knfusa.com/applications/oem/>.
[6] P.K. Das, A.B.M.T. Hasan, Mechanical micropumps and their applications: a review, AIP Conf. Proc. 1851 (1) (2017) 020110.
[7] D.J. Laser, J.G. Santiago, A review of micropumps, J. Micromech. Microeng. 14 (6) (2004) R35.
[8] A. Fridman, Plasma Chemistry, Cambridge University Press, New York, NY, 2008.
[9] Y. Yang, Y.I. Cho, A. Fridman, Plasma Discharge in Liquid: Water Treatment and Applications, CRC Press, Boca Raton, FL, 2012.
[10] S.E. Gilliland, M.L. Speck, Inactivation of microorganisms by electrohydraulic shock, Appl. Microbiol. 15 (5) (1967) 1031–1037.
[11] A. Melander, A. Delic, A. Björkblad, P. Juntunen, L. Samek, L. Vadillo, Modelling of electro hydraulic free and die forming of sheet steels, (in English), Int. J. Mater. Form. 6 (2) (2013) 223–231, 2013/06/01.
[12] Y. Yang, A. Gutsol, A. Fridman, Y.I. Cho, Removal of $CaCO_3$ scales on a filter membrane using plasma discharge in water, Int. J. Heat Mass Transf. 52 (21–22) (2009) 4901–4906.
[13] J. Harrison, D.L. Morris, J. Haynes, A. Hitchcock, C. Womack, D.C. Wherry, Electrohydraulic lithotripsy of gall stones–in vitro and animal studies, Gut 28 (3) (1987) 267–271.
[14] Servometer, "Electroformed Metal bellows," Servometer, Ed., ed. Cedar Grove, NJ: Servometer, 2015.
[15] S. Mededovic, B.R. Locke, Primary chemical reactions in pulsed electrical discharge channels in water, J. Phys. D Appl. Phys. 40 (24) (2007) 7734.
[16] G.S. Settles, Schlieren and Shadowgraph Techniques, first ed., Springer-Verlag, Berlin Heidelberg, New York, 2001.
[17] F.J. Gordillo-Vázquez, M. Camero, C. Gómez-Aleixandre, Spectroscopic measurements of the electron temperature in low pressure radiofrequency $Ar/H_2/C_2H_2$ and $Ar/H_2/CH_4$ plasmas used for the synthesis of nanocarbon structures, Plasma Sources Sci. Technol. 15 (1) (2006) 42.
[18] F.O. Borges, G.H. Cavalcanti, A.G. Trigueiros, Determination of plasma temperature by a semi-empirical method, Braz. J. Phys. 34 (2004) 1673–1676.
[19] G.B. Sretenović, I.B. Krstić, V.V. Kovačević, B.M. Obradović, M.M. Kuraica, Spectroscopic measurement of electric field in atmospheric-pressure plasma jet operating in bullet mode, Appl. Phys. Lett. 99 (16) (2011).
[20] J. Lubbers, R. Graaff, A simple and accurate formula for the sound velocity in water, Ultrasound Med. Biol. 24 (7) (1998) 1065–1068, 9.
[21] S. Katsuki, K. Tanaka, T. Fudamoto, T. Namihira, H. Akiyama, H. Bluhm, Shock waves due to pulsed streamer discharges in water, Jpn. J. Appl. Phys. 45 (1R) (2006) 239.
[22] W. An, K. Baumung, H. Bluhm, Underwater streamer propagation analyzed from detailed measurements of pressure release, J. Appl. Phys. 101 (5) (2007) 053302.
[23] J.E. Sansonetti, W.C. Martin, Handbook of Basic Atomic Spectroscopic Data, Gaithersburg, MD: National Institute of Standards and Technology, 2014. Available: <http://www.nist.gov/pml/data/handbook/>.
[24] A. Kramida, Y. Ralchenko, J. Reader, N.A. Team, NIST Atomic Spectra Database (version 5.3) [Online]. Available: <http://physics.nist.gov/asd>.
[25] A.M. Anpilov et al., Electric discharge in water as a source of UV radiation, ozone and hydrogen peroxide, J. Phys. D Appl. Phys. 34 (6) (2001) 993.
[26] Y. Yang, H. Kim, A. Fridman, Y.I. Cho, Effect of a plasma-assisted self-cleaning filter on the performance of PWT coil for the mitigation of mineral fouling in a heat exchanger, Int. J. Heat Mass Transf. 53 (1–3) (2010) 412–422.